International Journal of Smart Grid (IJSmartGrid)
https://www.ijsmartgrid.org/ Online ISSN: 2602-439X
A. Soeprijanto et al., Vol. 10, No. 1, March, 2026 Research Article

Redefinition of Transient Stability Boundaries for Overcurrent Relay Settings in Multi-Machine Power Systems with VSG Penetration

Adi Soeprijanto*, Ardyono Priyadi*, Dimas Fajar Uman Putra*, Dani Irfani*
Ony Asrarul Qudsi**, Naoto Yorino***

* Department of Electrical Engineering, Institut Teknologi Sepuluh Nopember, Surabaya 60111, Indonesia

** Department of Electrical Engineering, Politeknik Elektronika Negeri Surabaya, Surabaya 60111, Indonesia

*** Graduate School of Advanced Science and Engineering, National Institute of Technology(KOSEN) Kure College, Kure, Japan

(adisup@its.ac.id, priyadi@ee.its.ac.id, dimasfup@its.ac.id, irfanidani8@gmail.com, ony@pens.ac.id, yorino@hiroshima-u.ac.jp)

‡Corresponding Author; Adi Soeprijanto, Buildings A, B, C, and AJ, ITS Campus, Sukolilo, Surabaya 60111, Indonesia, Tel: (+6231) 5994251-54, Ext. 1206,

adisup@its.ac.id

Received: 11.12.2025 Accepted:08.02.2026

Abstract- VSG penetration can affect transient stability in power systems. CCT is the time limit set in OCR to isolate faults and serves as the boundary for power system stability during disturbances. VSG penetration may alter the CCT value, necessitating careful consideration of whether the OCR settings align with system stability boundary. This paper proposes a CCT calculation using the CT method due to VSG penetration. CT is determined through a numerical iteration process based on critical synchronization conditions due to VSG penetration in the power system. This method is sufficiently accurate for CCT calculation in complex systems. VSG penetration is modeled into a multi-machine system to provide a comprehensive view of transient stability. Subsequently, CCT is used as a boundary redefinition for OCR settings. Finally, an investigation is conducted on a modified IEEE 30-bus system, showing changes in transient stability boundary due to VSG penetration, indicating that OCR settings must be adjusted according to stability requirements to ensure the system remains stable after fault clearance. Quantitative validation shows that the proposed modified CT-based approach achieves an accuracy of 99.98% when compared with time-domain simulation–based reference results, demonstrating its high reliability in estimating the transient stability boundary.

Keywords-VSG, Transient Stability, CCT, Critical Trajectory, OCR setting.

1. Introduction

Authors should any word processing software that is Transient stability is a fundamental aspect that must be ensured in the operation of modern power systems, particularly when the system is subjected to large and sudden disturbances such as short circuits, transmission line outages, or protection device failures [1]. Transient stability refers to the ability of a power system to maintain rotor angle synchronism following the clearance of a large

Cite this article as: A. Soeprijanto, A. Priyadi, D. F. U. Putra, D. Irfani, O. A. Qudsi, and N. Yorino, "Redefinition of Transient Stability Boundaries for Overcurrent Relay Settings in Multi-Machine Power Systems with VSG Penetration" *International Journal of Smart Grid (ijSmartGrid)*, Vol. 10, No. 1, pp. 60-72, March, 2026.

disturbance within a specified time interval. In conventional power systems dominated by synchronous generators (SGs), transient stability studies primarily focus on the electromechanical interactions among synchronous machines through the transmission network.

However, the ongoing transition toward power systems with high penetration of renewable energy sources (RESs) has significantly altered system dynamic characteristics [2]. Large-scale integration of inverter-based RESs introduces increased uncertainty, reduced natural inertia, and control dynamics that differ fundamentally from those of conventional synchronous machines [3], [4]. Recent studies have shown that increasing RES penetration requires power systems to exhibit enhanced flexibility and resilience against large disturbances, particularly with respect to transient stability and protection coordination in modern power systems [5]-[7].

In response to these challenges, grid-forming inverters (GFMIs) have been developed to enable inverter-based resources to actively contribute to system stability. Among various GFMI approaches, the virtual synchronous generator (VSG) concept has attracted significant attention due to its capability to emulate the dynamic behavior of synchronous generators through the implementation of virtual inertia, a virtual governor, and a virtual automatic voltage regulator (AVR) [8]-[10]. This approach has been reported to improve frequency stability, voltage stability, and overall dynamic performance of power systems under various disturbance scenarios [11]-[13].

Despite these advancements, the majority of existing VSG-related studies primarily focus on small-signal stability, load fluctuations, or frequency stability, whereas comprehensive investigations of transient stability under large disturbances remain relatively limited [14]-[17]. Several recent works have begun to examine the impact of VSG penetration on transient stability using metrics such as the critical clearing angle (CCA) and the critical clearing time (CCT) [18]-[21]. Among these metrics, CCT is of particular practical relevance, as it directly relates to the allowable operating time of protection devices especially overcurrent relays (OCRs) and therefore plays a crucial role in real-world power system implementation and protection design [22].

Nevertheless, two major limitations can be identified in the existing literature. First, most CCT analyses associated with VSG penetration are conducted using single-machine infinite bus (SMIB) models, which are insufficient to capture the complex interactions among multiple machines and realistic network configurations. In practice, the impact of VSG penetration on transient stability strongly depends on the penetration location, network topology, and inter-machine interactions. Second, variations in CCT resulting from VSG penetration are rarely linked quantitatively to adjustments of OCR settings, leaving the practical implications for protection coordination largely unexplored.

In practical studies, CCT is commonly determined through time-domain simulations based on trial-and-error procedures or numerical fitting, which only provide approximate stability margins without yielding a precise stability boundary [23]. To address this limitation, several direct methods for CCT computation have been proposed, including the boundary controlling unstable equilibrium point (BCU) method and the critical trajectory (CT) method [24]-[27]. The BCU method, which is based on transient energy functions, enables direct computation of CCT but is applicable only to limited classes of power system models. In contrast, the CT method offers greater flexibility and can be applied to more detailed power system models, including multi-machine systems [28]-[30]. However, conventional CT formulations are not designed to accommodate the nonlinear control dynamics and operational characteristics of VSGs, necessitating further modifications to ensure applicability to modern power systems with significant GFMI penetration.

Motivated by these research gaps, this paper aims to develop and apply a modified CT-based approach to quantitatively analyze the impact of VSG penetration on the transient stability of multi-machine power systems. The CCT is computed through numerical integration of the nonlinear differential equations governing system dynamics before, during, and after fault clearance. The transient stability boundary is identified using a loss-of-synchronization (LOS) criterion defined with respect to the center of inertia (COI), enabling critical trajectory analysis for both SGs and VSGs within a unified multi-machine framework. The resulting CCT values are subsequently employed as quantitative stability limits for the determination and optimization of OCR settings with inverse definite minimum time (IDMT) characteristics, which are well suited for complex power systems with high levels of RES penetration [31].

As summarized in Table 1, existing studies either investigate VSG dynamic behavior without providing quantitative critical clearing time boundaries or address CCT estimation without explicitly considering grid-forming inverter dynamics and protection coordination. This paper uniquely integrates these aspects by establishing a CCT-based transient stability boundary for overcurrent relay settings in multi-machine power systems with virtual synchronous generator penetration.

The main contributions of this paper can be summarized as follows:

1. Providing guidelines for OCR settings based on the transient stability boundary of power systems under VSG penetration.

2. CCT calculation and system analysis due to VSG penetration are performed using the CT method to determine the system's stability boundary during faults.
3. The transient stability analysis mechanism of power systems due to VSG penetration is modeled using a multi-machine model, taking into account the network configuration with reference to the COI.

This paper is organized as follows. Section 2 describes the VSG penetration model in a multi-machine system. Section 3 explains the problem formulation for the quantitative calculation of CCT and transient stability boundary redefinition for OCR settings. Section 4 presents the simulation results with several test cases on the modified IEEE 30-bus system. Finally, Section 5 provides the conclusion of the paper.

2. System Modelling

2.1. VSG System Modelling

The topology of the VSG system is shown in Fig. 1. The active current in the VSG generates active power P, while the reactive current in the VSG generates reactive power Q. In this study, the transient stability analysis is confined to the inertial response time frame immediately following a large disturbance, during which the system dynamics are dominated by pure virtual inertia emulation of the VSG, while the effects of current limiting, converter saturation, control mode transitions, and primary or higher-level control actions are not considered due to their inherently slower response times [32]. Table 2 presents the VSG parameters used.

Table 1. Comparison of existing studies and the proposed approach

Ref	Power System Model	VSG Penetration Analysis	Transient Stability Evaluation	CCT Determination Method	Protection System Integration
[1]	Weak grid, inverter-dominated system	Yes (IBR-based RES)	Small-signal and dynamic stability	Not considered	No
[2]	Hybrid system (SG + grid-forming devices)	Yes	Time-domain transient stability	Not explicitly addressed	No
[3]	Inverter-intensive hybrid power plant	Yes	Small-signal stability	Not considered	No
[4]	Power system with AGC	Yes (VSG-based RES)	Frequency stability	Not considered	No
[8]	Parallel SG-VSG system with induction motor loads	Yes	Transient voltage stability	Not considered	No
[9]	Review of VSG models	Yes	Not specifically evaluated	Not considered	No
[10]	Single VSG-based system	Yes	Transient stability (controller-oriented)	Not considered	No
[14]	Single-machine VSG system	Yes	Frequency stability	Not considered	No
[15]	SG-VSG system	Yes	Low-frequency oscillation analysis	Not considered	No
[16]	Multi-VSG system	Yes	Transient stability	Not explicitly addressed	No
[19]	Parallel current-controlled VSCs and VSGs	Yes	Transient stability and current injection behavior	Not explicitly addressed	No
[20]	Single VSG-based system	Yes	Transient stability	Not considered	No
[21]	Grid-forming converter-based system	Yes (GFMI)	Transient stability	Yes (CCT)	No
[22]	Active distribution network with DERs	Not VSG-specific	Stability-constrained analysis	Not considered	Yes (OCR setting)
In this paper	Multi-machine power system	Yes (penetration level and location considered)	Transient stability under large disturbances	Yes (Critical Trajectory method)	Yes (OCR IDMT setting based on CCT)

The active power and reactive power generated by the VSG can be formulated according to equations (1) and (2).

$$P = \frac{V_g V_{VSG}}{X_L} \sin\delta \quad (1)$$

$$Q = \frac{V_{VSG}(V_{VSG} - V_g \cos\delta)}{X_L} \quad (2)$$

The VSG control system consists of the swing equation and the electromagnetic equation, which can be expressed by equations (3).

$$J\omega \frac{d^2\delta}{dt^2} = P_{rated} - P \quad (3)$$

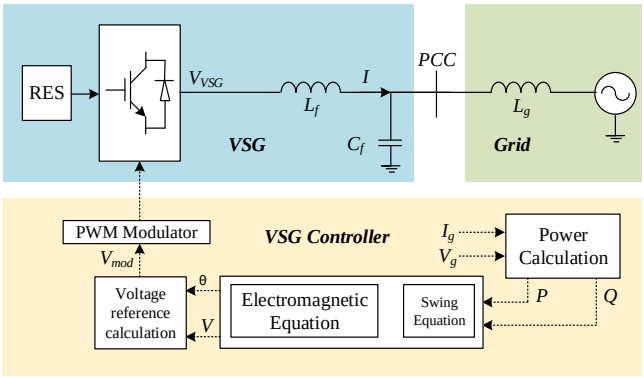

Fig. 1. VSG system topology.

By substituting equation (1) into equation (3), equation (4) is obtained.

$$J\omega \frac{d^2\delta}{dt^2} = P_{rated} - \frac{V_g V_{VSG}}{X_L} \sin\delta \quad (4)$$

Table 2. Main Parameters of VSG Used in Simulation

Parameter	Unit	VSG 1	VSG 2	VSG 3	VSG 4
P_{rated}	*MW*	30	20	25	20
Q_{rated}	*MVAR*	25	20	15	20
V_{VSG}	*p.u.*	1.082	1.082	1.082	1.082
X_L	*p.u.*	0.184	0.184	0.184	0.184
J	*p.u.*	2.5	2.5	2.5	2.5

2.2. Fault Condition of VSG

The transient stability of the system is assessed based on the conditions before the fault occurs, during the fault, and after the fault is cleared. Fig. 2 shows the equivalent circuit of the system for these three conditions. V_L is the voltage drop across the network, with $V_L = V_{VSG} - V_g$. X_g consisting of X_{g1} and X_{g2}. The superscripts ' and " represent the during-fault and post-fault conditions, respectively. Based on Fig. 3(a), there is a difference in the value of X_g in the pre-fault, during-fault, and post-fault conditions ($X_g' < X_g < X_g''$), which affects the voltage and current in the system, as shown in the phasor diagram in Fig. 3(b). From Fig. 3, V_{VSG} and I can be formulated according to equations (5) and (6).

$$V_{VSG} = I(X_L + X_g) + V_g \quad (5)$$

$$I = \frac{V_{VSG} - V_g}{X_L + X_g} \quad (6)$$

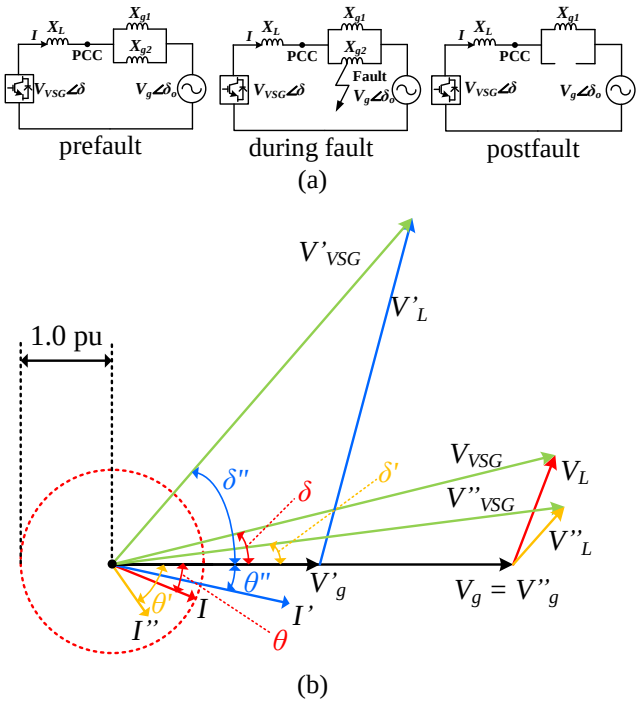

Fig 2. System condition (a) equivalent circuit for prefault, during fault, and postfault; (b) phasor diagram for prefault, during fault, and postfault.

2.3. Multi-machine Models

The equivalent circuit model of the generation system, network, and load is shown in Fig. 3. The rotor angle of each machine, including the VSG, depends on the terminal voltage and internal reactance. The machine terminal voltage and the PCC VSG voltage are obtained through the power flow iteration process.

To reduce complexity, a reduction is performed to simplify the analysis and mathematical calculations. In this research, Kron reduction is used to eliminate the load bus from the admittance matrix. The subscript n denotes the bus number, while the subscripts i and p represent the generator bus and the location of VSG penetration, respectively.

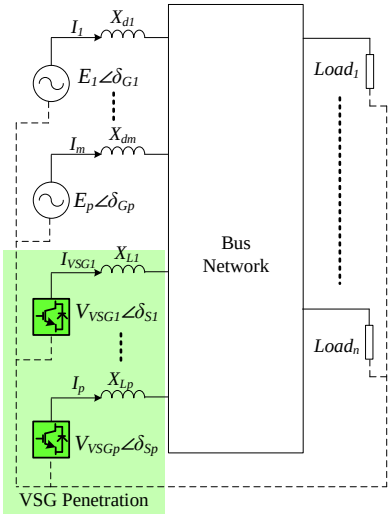

Fig. 3. Representation of multimachines system.

Thus, a complex multi-machine system is simplified according to the following equations:

$$\begin{bmatrix} Y_{11} & \cdots & Y_{1(n-1)} & Y_{1k} & Y_{1p} \\ \vdots & \ddots & \vdots & \vdots & \vdots \\ Y_{(n-1)1} & \cdots & Y_{(n-1)(n-1)} & Y_{nk} & Y_{np} \\ Y_{k1} & \cdots & Y_{kn} & Y_{kk} & Y_{kp} \\ Y_{p1} & \cdots & Y_{pn} & Y_{pk} & Y_{pp} \end{bmatrix} \textit{yields} \begin{bmatrix} Y_{11} & \cdots & Y_{1(n-1)} \\ \vdots & \ddots & \vdots \\ Y_{(n-1)1} & \cdots & Y_{(n-1)(n-1)} \end{bmatrix} \quad (7)$$

3. Problem Formulation of Proposed Method

CCT is the system stability boundary to be determined in this research. Quantitatively, CCT is calculated through a numerical iteration process based on CT with an end point at LOS. CCT lies between the ST and UT after the fault is cleared. The steps involved in the CCT calculation process are shown in Fig. 4. The procedure starts with system data initialization, including generator, network, and load parameters, followed by steady-state power flow calculation. Kron matrix reduction is then applied to obtain the reduced network model for transient analysis. The initial state variables before fault occurrence are determined, and a three-phase fault is introduced to evaluate system dynamics. The critical clearing time (CCT) is computed using a modified Critical Trajectory (CT) method by numerically integrating the nonlinear differential equations and identifying the loss-of-synchronization (LOS) condition based on the center-of-inertia reference. Finally, the obtained CCT is employed as a quantitative stability boundary for redefining overcurrent relay (OCR) settings, ensuring that relay operation time does not exceed the transient stability limit.

The proposed CT-based approach requires numerical integration of system differential equations combined with a limited number of trajectory iterations to identify the critical clearing time. Compared to conventional trial-and-error time-domain scanning, the method significantly reduces computational effort by directly converging toward the stability boundary.

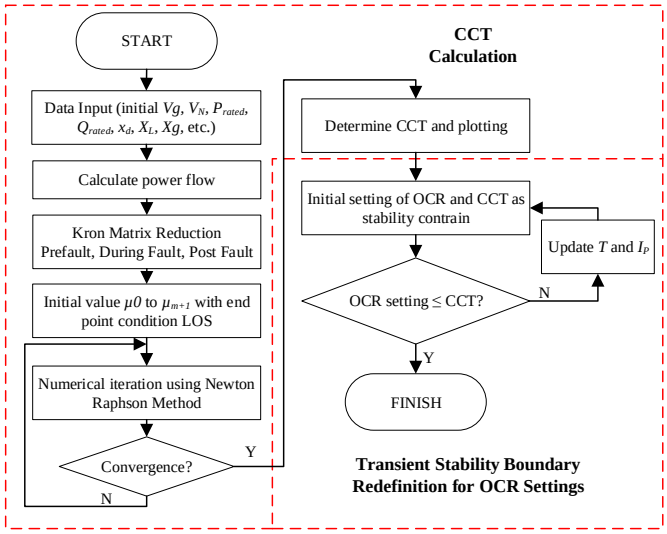

Fig. 4. Procedure of transient stability boundary redefinition for OCR settings.

The convergence behavior is robust, as the iteration process terminates once the LOS criterion is reached, and no sensitivity to initial guesses was observed in the conducted studies. Furthermore, the proposed approach is well suited for protection setting, as individual fault scenarios can be evaluated independently and executed in parallel, making the method scalable for larger power systems and multiple contingency assessments as demonstrated in [29] and [30].

3.1. COI Reference with VSG Penetration

The concept of COI is employed in this study to represent the collective behavior of all generators in the system as a single inertia mass, providing a more realistic approach to analyzing the dynamic interactions between generators during transient conditions. P_e in the bus network must be calculated first. This electrical power flow is based on the power generated by the SG and VSG. To prevent the SG and VSG from losing synchronization in the multi-machine system, the angles δ of the SG and VSG must follow the P_{COI} reference. P_{COI} is expressed according to the following equation:

$$P_{COI} = \left(\sum_{i=1}^{n} P_{mi} - P_{ei}(\delta_i)\right) + \left(\sum_{p=1}^{n} P_{mp} - P_{ep}(\delta_p)\right) \quad (8)$$

Using the COI concept, the swing equation with respect to the COI reference is as follows:

$$M_{(i+p)} \frac{d^2\delta_{(i+p)}}{dt^2} = \left(P_{mi} + P_{mp}\right) - \left(P_{ei} + P_{ep}\right) - \frac{M_{(i+p)}}{M_T} P_{COI} \quad (9)$$

M is the constant inertia of both the SG and VSG, which is the product of the moment of inertia J and the angular velocity ω. M_T is the total moment of inertia, calculated

using the following equation:

$$M_T = \left(\sum_{i=1}^{n} M_i\right) + \left(\sum_{p=1}^{n} M_p\right) \tag{10}$$

3.2. Critical Condition of the System

The CT method end point condition is LOS. According to reference [29], the LOS in a multi-machine system can be expressed by the following equation:

$$\begin{cases} \left[\dfrac{\partial P}{\partial \delta}\right].v \\ v \neq 0 \end{cases} \tag{11}$$

v is the eigenvector associated with the zero eigenvalue of the matrix $[\partial P/\partial \delta]$. As shown in Fig. 5, μ_u represents the end point based on LOS. By maintaining the value of μ_u as the end point condition, numerical iteration is then performed with the initialization of δ_0 and ω_0, starting from the pre-fault condition to the post-fault condition, as the network configuration changes during the fault. δ_0 and ω_0 can be calculated using equations (12) and (13).

$$\delta_0 = \frac{1}{M_T}\left(\sum_{i=1}^{n} M_i \delta_i + \sum_{p=1}^{n} M_p \delta_p\right) \tag{12}$$

$$\omega_0 = \frac{1}{M_T}\left(\sum_{i=1}^{n} M_i \omega_i + \sum_{p=1}^{n} M_p \omega_p\right) \tag{13}$$

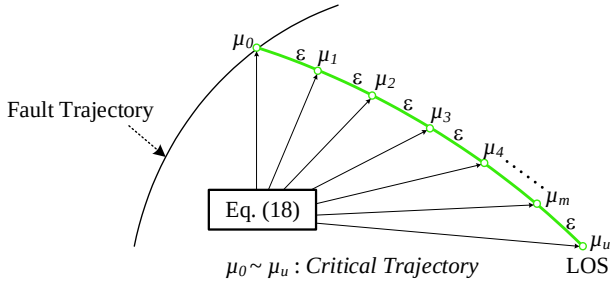

Fig. 5. Fault trajectory after fault clearing.

The pair δ_0 and ω_0 in equations (12) and (13) are nonlinear functions of a second-order differential equation. This function can be expressed by the following equation:

$$\mu = f(\mu, \mu_0, t) \tag{14}$$

Represented as a matrix with dimensions ($2n$+1),

$$\mu = [\delta_1, \omega_1, \delta_2, \omega_2, ..., \delta_n, \omega_n] \tag{15}$$

Numerical iteration is performed until the end point condition is reached, as shown in the following equation:

$$\mu_k = \mu_{k+1} - \mu_k - \frac{\dot{\mu}_{k+1} + \dot{\mu}_k}{\left|\dot{\mu}_{k+1} + \dot{\mu}_k\right|}\varepsilon \tag{16}$$

Where $\mathcal{E}$ is the distance between the two points of μ.

3.3. Iterative CCT Calculation Based on CT

The fault trajectory is obtained during the disturbance period [0,τ]. The fault trajectory can be expressed by the following equation:

$$\dot{\mu} = f(\mu); 0 \le t \le \tau; \mu(0) = \mu \tag{17}$$

$$\mu(t) = \chi(t; \mu); 0 \le t \le \tau \tag{18}$$

When the fault is cleared at time τ, the dynamic change in the trajectory becomes:

$$\dot{\mu} = f(\mu), \tau \le t \le \infty; f : R_N \to R_N \tag{19}$$

After the fault is cleared, the post-fault trajectory can be expressed by the following equation:

$$\mu(t) = \chi(t; \mu_0), \tau \le t \le \infty; \chi(\cdot; \mu_0 : R_N \to R_N) \tag{20}$$

CCT is determined based on the post-fault trajectory when the fault is cleared at time τ under the following conditions:

$$\mu_0 = \chi_F(\tau; \mu_{pre}), \tau = CCT \tag{21}$$

3.4. Transient Stability Boundary Redefinition for OCR Settings Based on CCT

The settings are configured by combining the standard inverse curve and the definite time curve. The key parameters in OCR settings are I_P and TSM [33]. In the IDMT characteristic, I_P and TSM are interrelated for OCR configuration, thus the transient stability boundary redefinition problem is represented by the following equation:

$$Minimize \to \sum_{f=1}^{f_{max}}\left(\sum_{i=1}^{n} T_i\right) \tag{22}$$

I_P can be determined according to the following constraints:

$$1.1 I_{FLi} \le I_{Pi} \le \alpha I_{FMi} \tag{23}$$

with,

$$\begin{cases} \alpha = 0.6 \to 0.6 I_{FMi} \ge 1.1 I_{FLi} \\ \alpha = 0.8 \to otherwise \end{cases} \tag{24}$$

Meanwhile, TSM is determined based on the following equation:

$$T_i = \frac{0.14}{\left(I_{Fi}/I_{Pi}\right)^{0.02} - 1} TSM_i \quad (25)$$

To solve the transient stability boundary redefinition problem in equation (24), CCT is used as the constraint for the settings. Thus, the OCR operating time can be expressed by the following equation:

$$T_i \leq CCT \quad (26)$$

4. Case Study, Result, and Analysis

The test case system is conducted on the modified IEEE 30-bus system with VSG penetration [34]. The penetration locations are shown in Fig. 6. There are ten three-phase ground fault points (A, B, C, D, E, F, G, H, I, and J) for investigation and analysis. The faults occur on transmission lines located near buses. For example, fault point "E" occurs on the line between bus 2 and bus 6, with the fault location near bus 2. Subsequently, transient stability boundary redefinition for OCR settings are applied to the OCR closest to the fault point on the transmission line, as illustrated in Fig. 7.

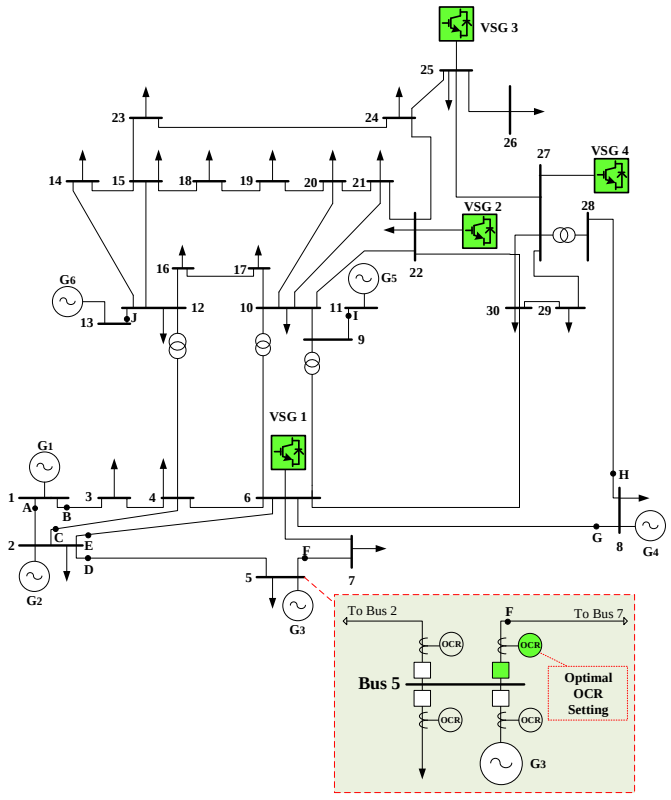

Fig. 6. Modified IEEE 30 bus systems with VSG penetration.

Based on Fig. 7, five test cases are used for VSG penetration as follows:

- *Test case 1*: VSG 1, VSG 2, VSG 3, and VSG 4 are penetrated.
- *Test case 2*: VSG 2, VSG 3, and VSG 4 are penetrated.
- *Test case 3*: VSG 1, VSG 3, and VSG 4 are penetrated.
- *Test case 4*: VSG 1, VSG 2, and VSG 4 are penetrated.
- *Test case 5*: VSG 1, VSG 2, and VSG 3 are penetrated.

CCT and transient stability boundary redefinition for OCR settings are provided in Tables II-VI. The proposed modified CT method for CCT calculation is compared with the TDS method, based on numerical fitting of τ. For example, the CCT value "0.84-0.85" at fault point "I" in Table II indicates that the system will remain stable if ST with τ_s = 0.84s and will become unstable if UT with τ_u = 0.85s. This serves as a reference for determining whether the CCT obtained through the CT method is accurate in determining CCT. Subsequently, the CCT is used as a boundary for setting the OCR to achieve the transient stability boundary redefinition for OCR setting.

4.1. Existing Condition Without VSG Penetration

In the existing condition without VSG penetration, CCT values and OCR settings with transient stability limits for each fault point are obtained, as shown in Table 3. Based on the data in Table 1, the average accuracy of the CCT calculated using the proposed method is 99.93%. The CCT obtained for each fault point is used for OCR settings. These OCR settings serve as the initial OCR configuration before redefinition is performed due to VSG penetration.

Table 3. CCT and OCR setting of modified IEEE 30 bus system without VSG penetration

Fault	CCT Calculation			Existing OCR Setting		
	ST - UT (s)	CT (s)	Accuracy (%)	TSM	I_P	T (s)
A	0.50-0.51	0.5011	100%	4.4	8.80	0.425
B	0.51-0.52	0.5129	100%	2.5	3.15	0.475
C	0.62-0.63	0.6281	100%	3.2	2.35	0.550
D	0.62-0.63	0.6238	100%	3.4	2.66	0.550
E	0.62-0.63	0.6289	100%	3.8	2.78	0.550
F	1.33-1.34	1.3423	99.83%	1.1	4.77	1.250
G	1.43-1.44	1.4473	99.49%	1.6	8.07	1.300
H	1.67-1.68	1.6780	100%	0.4	1.37	1.525
I	0.97-0.98	0.9764	100%	1.7	5.07	0.850
J	1.03-1.04	1.0388	100%	1.9	5.41	0.950

4.2. Transient Stability Analysis and Redefinition OCR Setting due to VSG Penetratition

VSG penetration impacts the system's stability boundary, which will change depending on the location of VSG penetration. The study conducted on test cases 1-5 shows changes in CCT as a stability boundary. The CCT at

fault points "A", "B", and "H" in test cases 1, 3, 4, and 5 is greater than the CCT in the existing condition at the same fault points. Meanwhile, in test case 2, the CCT at fault points "A", "B", "G", and "H" is greater than the CCT in the existing condition at the same fault points. Thus, the transient stability boundary redefinition for OCR setting can remain the same as in the existing condition when the CCT due to VSG penetration is larger, as the system stability becomes greater than in the existing condition. However, at other fault points, redefinition is required because the CCT changes with stability limits lower than those in the existing condition.

- *Test Case 1*

In test case 1, there is a penetration of VSG 1 with a capacity of 30 MW, VSG 2 with a capacity of 20 MW, VSG 3 with a capacity of 25 MW, and VSG 4 with a capacity of 20 MW, resulting in a total VSG penetration capacity of 27% in the system. The CCT and redefinition for OCR settings are shown in Table 4. The average accuracy of the proposed method for CCT calculation in test case 1 is 100%.

Table 4. CCT and redefinition OCR setting of modified IEEE 30 bus system in Test Case 1

Fault	CCT Calculation			Redefinition OCR Setting		
	ST - UT (s)	CT (s)	Accuracy (%)	TSM	I_P	T (s)
A	0.84-0.85	0.8437	100%	4.4	8.80	0.425
B	0.85-0.86	0.8567	100%	2.5	3.15	0.475
C	0.62-0.63	0.6251	100%	8.9	5.22	0.55
D	0.62-0.63	0.6229	100%	5.2	5.02	0.5
E	0.62-0.63	0.6256	100%	5.2	6.38	0.5
F	0.97-0.98	0.9711	100%	3.7	10.15	0.9
G	0.80-0.81	0.8063	100%	3.7	18.08	0.775
H	1.74-1.75	1.7400	100%	0.4	1.37	1.525
I	0.84-0.85	0.8419	100%	2.3	10.94	0.75
J	0.85-0.86	0.8589	100%	2.7	11.53	0.775

- *Test Case 2*

In test case 2, there is a penetration of VSG 2 with a capacity of 20 MW, VSG 3 with a capacity of 25 MW, and VSG 4 with a capacity of 20 MW, resulting in a total VSG penetration capacity of 19% in the system. The CCT and redefinition OCR settings are shown in Table 5. The average accuracy of the proposed method for CCT calculation in test case 2 is 99.98%. Fig. 7 illustrates the difference in redefinition OCR settings with VSG penetration in test case 2 at fault location point "C" compared to the existing condition.

- *Test Case 3*

In test case 3, there is a penetration of VSG 1 with a capacity of 30 MW, VSG 3 with a capacity of 25 MW, and VSG 4 with a capacity of 20 MW, resulting in a total VSG penetration capacity of 21% in the system. The CCT and redefinition OCR settings are shown in Table 6. The average accuracy of the proposed method for CCT calculation in test case 3 is 100%.

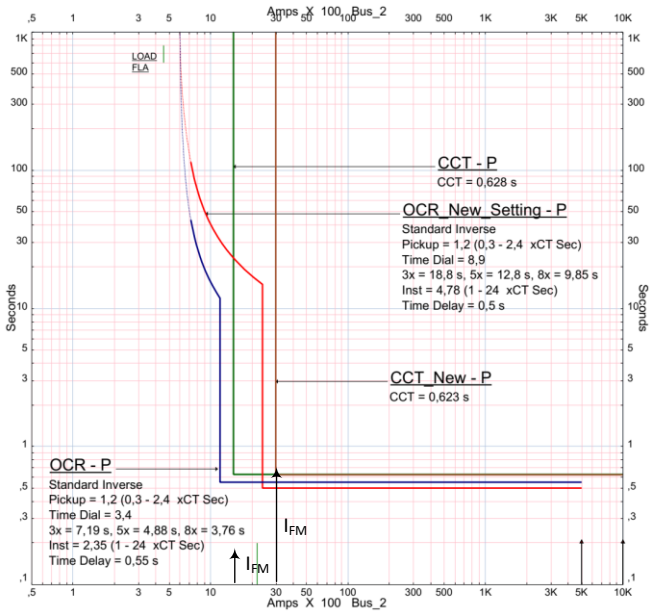

Fig. 7. Transient stability boundary redefinition for OCR Setting with VSG penetration in test case 2 at fault location point "C".

Table 5. CCT and redefinition OCR setting of modified IEEE 30 bus system in Test Case 2

Fault	CCT Calculation			Redefinition OCR Setting		
	TDS (s)	CT (s)	Accuracy (%)	TSM	I_P	T (s)
A	0.70-0.71	0.7087	100%	4.4	8.80	0.425
B	0.70-0.71	0.7095	100%	2.5	3.15	0.475
C	0.62-0.63	0.6227	100%	8.9	4.78	0.50
D	0.62-0.63	0.6203	100%	5.2	4.96	0.50
E	0.62-0.63	0.6227	100%	5.2	5.67	0.50
F	1.02-1.03	1.0290	100%	3.7	9.40	0.95
G	2.07-2.08	2.0850	99.76%	3.7	16.12	1.95
H	1.84-1.85	1.8440	100%	0.4	1.37	1.525
I	0.84-0.85	0.8453	100%	2.3	10.52	0.75
J	0.85-0.86	0.8530	100%	2.7	11.10	0.775

Table 6. CCT and redefinition OCR setting of modified IEEE 30 bus system in Test Case 3

Fault	CCT Calculation			Redefinition OCR Setting		
	TDS (s)	CT (s)	Accuracy (%)	TSM	I_P	T (s)
A	0.75-0.76	0.7561	100%	4.4	8.80	0.425
B	0.75-0.76	0.7513	100%	2.5	3.15	0.475
C	0.59-0.60	0.5975	100%	8.9	4.98	0.5
D	0.62-0.63	0.6203	100%	5.2	4.88	0.5
E	0.61-0.62	0.6155	100%	5.2	6.10	0.55
F	1.01-1.02	1.0126	100%	3.7	9.75	0.95
G	0.81-0.82	0.8110	100%	3.7	17.28	0.75
H	1.81-1.82	1.8162	100%	0.4	1.37	1.525
I	0.89-0.90	0.8980	100%	2.3	10.05	0.8
J	0.91-0.92	0.9165	100%	2.7	10.75	0.875

- *Test Case 4*

In test case 4, there is a penetration of VSG 1 with a capacity of 30 MW, VSG 2 with a capacity of 20 MW, and VSG 4 with a capacity of 20 MW, resulting in a total VSG penetration capacity of 20% in the system. The CCT and redefinition OCR settings are shown in Table 7. The average accuracy of the proposed method for CCT calculation in test case 4 is 99.999%.

- *Test Case 5*

In test case 5, there is a penetration of VSG 1 with a capacity of 30 MW, VSG 2 with a capacity of 20 MW, and VSG 3 with a capacity of 25 MW, resulting in a total VSG penetration capacity of 21% in the system. The CCT and redefinition OCR settings are shown in Table 8. The average accuracy of the proposed method for CCT calculation in test case 5 is 100%. Fig. 8 illustrates the difference in transient stability boundary redefinition for OCR settings with VSG penetration in test case 5 at fault location point "G" compared to the existing condition.

Table 7. CCT and redefinition OCR setting of modified IEEE 30 bus system in Test Case 4

Fault	CCT Calculation			Redefinition OCR Setting		
	TDS (s)	CT (s)	Accuracy (%)	TSM	I_P	T (s)
A	0.67-0.68	0.6784	100%	4.4	8.80	0.425
B	0.68-0.69	0.6850	100%	2.5	3.15	0.475
C	0.59-0.60	0.5900	100%	8.9	5.03	0.5
D	0.59-0.60	0.5915	100%	5.2	4.86	0.5
E	0.59-0.60	0.5902	100%	5.2	6.15	0.5
F	0.98-0.99	0.9880	100%	3.7	9.79	0.92
G	0.81-0.82	0.8200	100%	3.7	17.45	0.75
H	1.79-1.80	1.7899	99.99%	0.4	1.37	1.525
I	0.86-0.87	0.8602	100%	2.1	10.55	0.75
J	0.87-0.88	0.8784	100%	2.2	11.09	0.8

Table 8. CCT and redefinition OCR setting of modified IEEE 30 bus system in Test Case 5

Fault	CCT Calculation			Redefinition OCR Setting		
	TDS (s)	CT (s)	Accuracy (%)	TSM	I_P	T (s)
A	0.69-0.70	0.6994	100%	4.4	8.80	0.425
B	0.70-0.71	0.7042	100%	2.5	3.15	0.475
C	0.59-0.60	0.5912	100%	7.4	4.40	0.5
D	0.58-0.59	0.5892	100%	5.2	4.99	0.5
E	0.58-0.59	0.5896	100%	5.2	5.21	0.55
F	0.96-0.97	0.9640	100%	3.7	8.95	0.9
G	0.78-0.79	0.7896	100%	3.9	15.13	1.7
H	1.75-1.76	1.7557	100%	0.4	1.37	1.525
I	0.85-0.86	0.8565	100%	2.0	9.51	0.75
J	0.85-0.86	0.8589	100%	1.9	10.14	0.775

The radar diagram in Fig. 9 shows the changes in CCT due to VSG penetration in the modified IEEE 30-bus system. At certain fault locations, the CCT values increase, providing better stability boundary. However, at different fault locations, the CCT values decrease, leading to worse stability boundary. A closer examination reveals that the reduction in CCT values occurs at fault locations near the VSG penetration point. For instance, at fault location G in Test Case 2, where no VSG1 penetration is present, the CCT value increases compared to Test Cases 1, 3, 4, and 5 with VSG1 penetration. This phenomenon is attributed to the increased short-circuit current contribution at locations close to the VSG penetration, which consequently reduces the CCT as the transient stability boundary. This indicates that redefinition of the OCR settings is necessary to ensure the system remains stable after the fault is cleared.

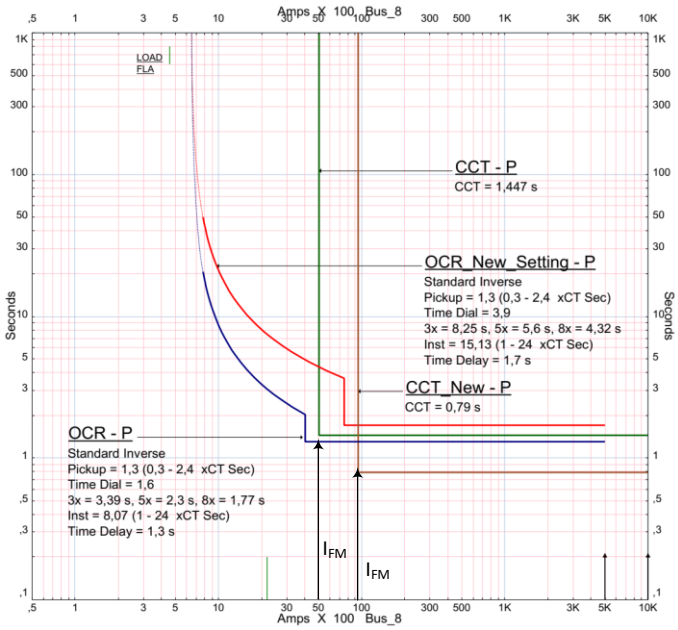

Fig. 8. Transient stability boundary redefinition for OCR Setting with VSG penetration in test case 5 at fault location point "G".

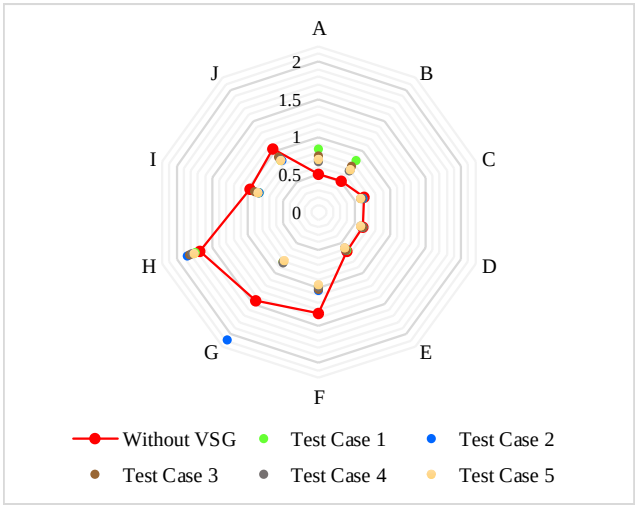

Fig. 9. CCT comparison of modified IEEE 30 bus systems with VSG penetration using Test Case 1-5 in "A" – "J" fault point.

Fig. 10 shows the angular velocity (ω) vs. angle (δ) curve for SG and VSG, which forms the trajectory. When the fault is cleared by opening the CB through OCR settings at $T = \tau_s$, the fault trajectory of each SG and VSG follows the stable trajectory "2." Conversely, when the fault is cleared by opening the CB through OCR settings at $T = \tau_u$, the fault trajectory of each SG and VSG follows the unstable trajectory "3." Trajectory "4" represents the stability boundary for SG and VSG, calculated based on the proposed modified CT method for redefinition OCR settings due to VSG penetration in the system. The proposed CT method lies between the stable trajectory and the unstable trajectory. Based on the data in Tables 3-8, the average accuracy of the proposed method is 99.98%. This indicates that the proposed method is accurate in assessing the impact of VSG penetration on system stability.

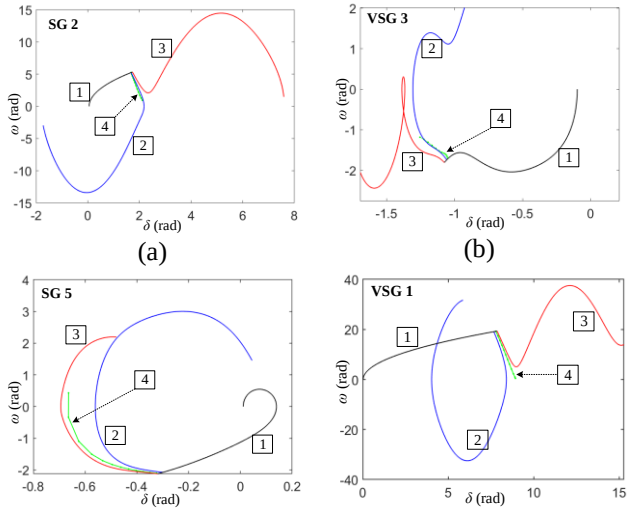

Fig. 10. Angular velocity (ω) vs angle (δ) curve of the SG and the VSG which representation trajectory of Modified IEEE 30 bus systems with Test Case 1 (a) SG 2 when fault occur in point "D", (b) VSG 3 when fault occur in point "D", (c) SG 5 when fault occur in point "G", (d) VSG 1 when fault occur in point "G".

The dynamic behavior of SG and VSG when the fault is cleared by the CB with redefinition OCR settings based on CCT calculation using the CT method can be seen in Fig. 11. The dynamic behavior of angle δ for SG 1-6 and VSG 1-4 during the fault at point "I" until the fault is cleared in test case 1 is shown in Fig. 11(a). When the fault is cleared with $T \leq$ CCT, the δ of each SG and VSG fluctuates but still demonstrates stable behavior, as the δ values for both SG and VSG fluctuate within certain limits. Similarly, the dynamic behavior of ω for SG and VSG in Fig. 11(b) shows that the ω fluctuations remain stable, as the dynamic behavior of ω for all generators and VSGs is within certain bounds. Fig. 11(c) shows the behavior of δ in SG 3 and VSG 1 when the fault is cleared at T = CCT and $T = \mu_u$. When the fault is cleared at T = CCT, the δ of SG 3 and VSG 1 demonstrates stable behavior. However, when the fault is cleared at $T = \mu_u$, the δ of SG 3 and VSG 1 increasingly moves in the negative direction. This indicates unstable behavior when the fault is cleared at $T = \mu_u$.

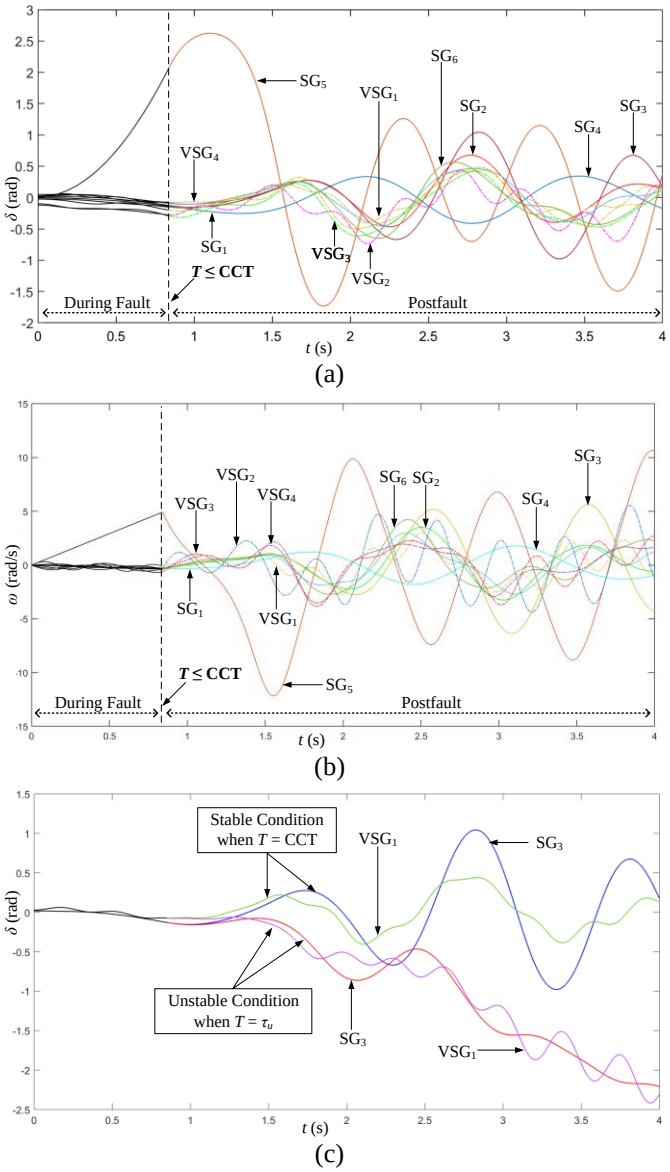

Fig. 11. Dynamic behavior of the SG 1-6 and the VSG 1-4 for fault in point "I" of Modified IEEE 30 bus systems with Test Case 1 when fault cleared in $T \leq$ CCT, (a) Angle (δ) behavior, (b) Angular velocity (ω) behavior, (c) Stable and unstable condition of the SG 3 and the VSG 1.

5. Conclusion

This study demonstrates that the CT method provides an accurate approach for determining the CCT in power systems with VSG penetration. Based on the data in Tables 3-8, the average accuracy of the proposed method is 99.98%. This indicates that the proposed method is accurate in assessing the impact of VSG penetration on system stability.

Changes in the system's stability boundary are evaluated based on variations in the CCT value due to VSG penetration, which are subsequently used as the basis for redefinition OCR settings. Simulation results have confirmed that the proposed method successfully achieves the primary objectives of analyzing transient stability and redefinition OCR settings in the presence of VSG penetration in power systems. If a fault is cleared within the CCT, the fault trajectory will oscillate around the stable equilibrium point, allowing the system to regain stability. However, if the fault is cleared beyond the CCT, the fault trajectory will exceed the stability limit, causing the system to become unstable. Therefore, this work provides a novel framework for assessing the impact of VSG integration, offering system stability analysis for modern power systems and paving the way for more resilient and sustainable grid operations.

Despite these contributions, several limitations should be acknowledged. The analysis is conducted under predefined VSG parameters and assumes idealized protection operation without considering delays, relay coordination, or adaptive protection schemes. Moreover, nonlinear effects such as converter saturation, detailed current-limiting behavior, and control mode transitions under severe faults are not explicitly modeled, which may influence the transient stability boundary in practical implementations. Future research will focus on extending the proposed framework to incorporate detailed VSG control nonlinearities, adaptive and communication-assisted protection strategies, and validation using larger-scale power systems and real-time simulation or hardware-in-the-loop platforms.

Acknowledgements

The authors would like to express their sincere gratitude to the Ministry of Education, Science, and Technology of the Republic of Indonesia for the support provided under contract number 017/C3/DT.05.00/PL/2025, which has greatly contributed to the completion of this research.

The authors used ChatGPT (OpenAI) to assist grammar improvements during manuscript preparation. All content has been reviewed and verified by the authors for accuracy and integrity.

Author Contributions

Adi Soeprijanto conceived and supervised the study; Ardyono Priadi and Dimas Fajar Uman Putra contributed to the methodology, system modeling, and analysis; Dani Irfani and Ony Asrarul Qudsi supported the investigation, validation, and data interpretation; Naoto Yorino provided technical review and critical revision of the manuscript. All authors have read and agreed to the published version of the manuscript.

Conflict of Interest

The author(s) declared no potential conflicts of interest with respect to the research, authorship, and/or publication of this article.

References

[1] M. I. Saleem, S. Saha, U. Izhar and L. Ang, “Stability assessment of inverter-based renewable energy sources integrated to weak grids”, IET Energy Syst. Integr., 1-20 (2024), https://doi.org/10.1049/esi2.12151.

[2] X. He, S. Pan and H. Geng, "Transient stability of hybrid power systems dominated by different types of grid-forming devices", IEEE Transactions on Energy Conversion, vol. 37, no. 2, pp. 868-879, June 2022, doi: 10.1109/TEC.2021.3113399.

[3] L. Ding, J. Zhang, X. Lu, S. Dong, A. Hoke and J. Tan, "Inverter intensive hybrid power plant modeling with small-signal stability augmentation through flexible operation mode transition", IEEE Journal of Emerging and Selected Topics in Power Electronics, doi: 10.1109/JESTPE.2024.3432850.

[4] W. Zhang, W. Sheng, Q. Duan, H. Huang and X. Yan, "Automatic generation control with virtual synchronous renewables," in Journal of Modern Power Systems and Clean Energy, vol. 11, no. 1, pp. 267-279, January 2023, doi: 10.35833/MPCE.2020.000921.

[5] M. Taghavi and C.J. Lee, “Development of a novel hydrogen liquefaction structure based on liquefied natural gas regasification operations and solid oxide fuel cell: Exergy and economic analyses”, Fuel, vol. 384, Art. no. 133826, 2025, doi: 10.1016/j.fuel.2024.133826.

[6] M. Taghavi, H.J. Yoon, J.-U. Choi, and C.J. Lee, “Innovative structure of a liquefied natural gas (LNG) process by mixed fluid cascade using solar renewable energy, photovoltaic panels, and absorption refrigeration system”, Computer Aided Chemical Engineering, vol. 53, F. Manenti and G. V. Reklaitis, Eds. Elsevier, 2024, pp. 2071–2076, doi: 10.1016/B978-0-443-28824-1.50346-X.

[7] M. Taghavi and C.J. Lee, “Development of novel hydrogen liquefaction structures based on waste heat recovery in diffusion–absorption refrigeration and power generation units”, Energy Conversion and Management, vol. 302, Art. no. 118056, 2024, doi: 10.1016/j.enconman.2023.118056.

[8] H. Cheng, W. Huang, C. Shen, Y. Peng, Z. Shuai and Z. J. Shen, "Transient voltage stability of paralleled synchronous and virtual synchronous generators with ınduction motor loads", IEEE Transactions on Smart

Grid, vol. 12, no. 6, pp. 4983-4999, Nov. 2021, doi: 10.1109/TSG.2021.3104655.

[9] A. Suvorov, A. Askarov, A. Kievets, and V. Rudnik, "A comprehensive assessment of the state-of-the-art virtual synchronous generator models," Electric Power Systems Research, vol. 209, pp. 108054, 2022, https://doi.org/10.1016/j.epsr.2022.108054.

[10] O.A. Qudsi, A.Soeprijanto, A. Priyadi, "Virtual inertia calculation and virtual power system stabiliser design for stability enhancement of virtual synchronous generator system under transient condition", IET Energy Syst. Integr. 6(S1), 903–917 (2024).https://doi.org/10.1049/esi2.12177.

[11] M. Taghavi, H. Salarian, and B. Ghorbani, "Thermodynamic and exergy evaluation of a novel integrated hydrogen liquefaction structure using liquid air cold energy recovery, solid oxide fuel cell and photovoltaic panels", Journal of Cleaner Production, vol. 320, Art. no. 128821, 2021, doi: 10.1016/j.jclepro.2021.128821.

[12] M. Taghavi, H. Salarian, and B. Ghorbani, "Economic evaluation of a hybrid hydrogen liquefaction system utilizing liquid air cold recovery and renewable energies", Renewable Energy Research and Applications, vol. 4, no. 1, pp. 125-143, 2023, doi: 10.22044/rera.2022.11899.1122.

[13] S. Ho and M. Taghavi, "Solar energy development: Study cases in Iran and Malaysia", International Journal of Engineering Trends and Technology, vol. 70, no. 8, pp. 408–422, 2022, doi: 10.14445/22315381/IJETT-V70I8P242.

[14] D. Li, Q. Zhu, S. Lin and X. Y. Bian, "A self-adaptive ınertia and damping combination control of vsg to support frequency stability", IEEE Transactions on Energy Conversion, vol. 32, no. 1, pp. 397-398, March 2017, doi: 10.1109/TEC.2016.2623982.

[15] H. Wang, Y. Hao, H. He, H. Dong, S. Lu, G. Zhang, J. Yang, and Z. Chen., "Influence mechanism and virtual power system stabiliser method of virtual synchronous generator for low−frequency oscillation of power system", IET Energy Syst. Integr. 6(2), 104–116 (2024). https://doi.org/10.1049/esi2.12119.

[16] L. Chen, J. Tang, X. Qiao, H. Chen, J. Zhu, Y. Jiang, Z. Zhao, R. Hu, and X. Deng, "Investigation on transient stability enhancement of multi-VSG system incorporating resistive SFCLs based on deep reinforcement learning", IEEE Transactions on Industry Applications, vol. 60, no. 1, pp. 1780-1793, Jan.-Feb. 2024, doi: 10.1109/TIA.2023.3321264.

[17] M. Taghavi, H. Salarian, and B. Ghorbani, "Thermodynamic and exergy evaluation of a novel integrated hydrogen liquefaction structure using liquid air cold energy recovery, solid oxide fuel cell and photovoltaic panels", Journal of Cleaner Production, vol. 320, Art. no. 128821, 2021, doi: 10.1016/j.jclepro.2021.128821.

[18] M. Taghavi, H. Salarian, and B. Ghorbani, "Economic evaluation of a hybrid hydrogen liquefaction system utilizing liquid air cold recovery and renewable energies", Renewable Energy Research and Applications, vol. 4, no. 1, pp. 125–143, 2023, doi: 10.22044/rera.2022.11899.1122.

[19] C. Shen, Z. Shuai, Y. Shen, Y. Peng, X. Liu, Z. Li, and Z. J. Shen, "Transient stability and current injection design of paralleled current-controlled VSCs and virtual synchronous generators", IEEE Transactions on Smart Grid, vol. 12, no. 2, pp. 1118-1134, March 2021, doi: 10.1109/TSG.2020.3032610.

[20] P. Ge, C. Tu, F. Xiao, Q. Guo and J. Gao, "Design-oriented analysis and transient stability enhancement control for a virtual synchronous generator", IEEE Transactions on Industrial Electronics, vol. 70, no. 3, pp. 2675-2684, March 2023, doi: 10.1109/TIE.2022.3172761.

[21] T. Qoria, F. Gruson, F. Colas, G. Denis, T. Prevost and X. Guillaud, "Critical clearing time determination and enhancement of grid-forming converters embedding virtual ımpedance as current limitation algorithm", IEEE Journal of Emerging and Selected Topics in Power Electronics, vol. 8, no. 2, pp. 1050-1061, June 2020, doi: 10.1109/JESTPE.2019.2959085.

[22] A. N. Sheta, B. E. Sedhom, A. Pal, M. S. E. Moursi and A. A. Eladl, "Stability-constrained settings of directional overcurrent relays with shifted user-defined characteristics for distribution networks with DERs", IEEE Transactions on Power Delivery, vol. 39, no. 4, pp. 2401-2413, Aug. 2024, doi: 10.1109/TPWRD.2024.3403921.

[23] M. N. Acosta, E. Gómez, F. Gonzalez-Longatt, M. A. Andrade, E. Vázquez and E. Barocio, "Single value decomposition to estimate critical clearing time of a power system using measurements", IEEE Access, vol. 9, pp. 125999-126010, 2021, doi: 10.1109/ACCESS.2021.3111006.

[24] T. L. Vu, S. M. Al Araifi, M. S. El Moursi and K. Turitsyn, "Toward simulation-free estimation of critical clearing time", IEEE Transactions on Power Systems, vol. 31, no. 6, pp. 4722-4731, Nov. 2016, doi: 10.1109/TPWRS.2016.2523265.

[25] Y. Liu, Z. Chen, H. Yao, L. Yi and Q. H. Wu, "Estimating critical clearing time of grid faults using DA of state-reduction model of power systems", CSEE Journal of Power and Energy Systems, vol. 10, no. 2, pp. 807-820, March 2024, doi: 10.17775/CSEEJPES.2022.07170.

[26] C. Mishra, "Critical clearing time sensitivity for differential-algebraic power system model," IEEE Transactions on Power Systems, vol. 36, no. 4, pp. 3153-3162, July 2021, doi: 10.1109/TPWRS.2020.3040625.

[27] S. Jiriwibhakorn, "Critical clearing time prediction for power transmission using an adaptive neuro-fuzzy ınference system", IEEE Access, vol. 11, pp. 142100-142110, 2023, doi: 10.1109/ACCESS.2023.3341968.

[28] S. Sharma, S. Pushpak, V. Chinde and I. Dobson, "Sensitivity of transient stability critical clearing time", IEEE Transactions on Power Systems, vol. 33, no. 6, pp. 6476-6486, Nov. 2018, doi: 10.1109/TPWRS.2018.2854650.

[29] N. Yorino, A. Priyadi, H. Kakui and M. Takeshita, "A new method for obtaining critical clearing time for transient stability", IEEE Transactions on Power Systems, vol. 25, no. 3, pp. 1620-1626, Aug. 2010, doi: 10.1109/TPWRS.2009.2040003.

[30] I. B. Sulistiawati, A. Priyadi, O. A. Qudsi, A. Soeprijanto and N. Yorino, “Critical clearing time prediction within various loads for transient stability assessment by means of the extreme learning machine method”, International Journal of Electrical Power & Energy Systems, Vol. 77, 2016, Pages 345-352, ISSN0142-0615, doi: 10.1016/j.ijepes.2015.11.034.

[31] P. Alaee and T. Amraee, "Optimal coordination of directional overcurrent relays in meshed active distribution network using ımperialistic competition algorithm", Journal of Modern Power Systems and Clean Energy, vol. 9, no. 2, pp. 416-422, March 2021, doi: 10.35833/MPCE.2019.000184.

[32] B. Tan, J. Zhao, M. Netto, V. Krishnan, V. Terzija, and Y. Zhang, “Power system inertia estimation: Review of methods and the impacts of converter-interfaced generations”, International Journal of Electrical Power & Energy Systems, vol. 134, Art. no. 107362, Jan. 2022, doi: 10.1016/j.ijepes.2021.107362.

[33] "IEEE guide for protective relay applications to power system buses", IEEE Std C37.234-2009 , vol., no., pp.1 125, 6 Nov. 2009, doi:10.1109/IEEESTD.2009.5325912.

[34] M. Shahidehpour and Y. Wang, "Appendix C: IEEE30 Bus System Data", Communication and control in electric power systems: applications of parallel and distributed processing, IEEE, 2003, pp.493-495, doi: 10.1002/0471462926.app3.